Materials Today Communications 30 (2022) 103007

Contents lists available at ScienceDirect

Materials Today Communications

journal homepage: www.elsevier.com/locate/mtcomm

In situ alloying of NiTi: Influence of laser powder bed fusion (LBPF) scanning strategy on chemical composition

Agnieszka Chmielewska [a,*], Bartłomiej Wysocki [b,c], Joseph Buhagiar [d], Bartosz Michalski [a], Bogusława Adamczyk-Cieślak [a], Michał Gloc [a], Wojciech Święszkowski [a]

[a] Faculty of Material Science and Engineering, Warsaw University of Technology, Woloska 141 Str, 02 507 Warsaw, Poland
[b] Center of Digital Science and Technology, Cardinal Stefan Wyszynski University in Warsaw, Woycickiego 1/3, 01–938 Warsaw, Poland
[c] Additive Manufacturing Research Center, College of Engineering, Youngstown State University, Youngstown, OH 44555, USA
[d] Department of Metallurgy and Materials Engineering, University of Malta, Msida, Malta

ARTICLE INFO

Keywords:
Nickel titanium (NiTi)
Nitinol
Laser powder bed fusion (LPBF)
Selective laser melting (SLM)
Remelting
Elemental powders
Pre-mixed powders

ABSTRACT

NiTi alloys are widely used in different industrial and medical applications. Due to the inherent difficulty in the machining of these alloys, the use of Additive Manufacturing (AM) methods has become a popular method for their production. When working with NiTi alloys, there is a requirement on the precise control of their chemical composition, as this determines the phase transition temperatures which are responsible for their shape memory or superelastic behaviour. The high energies used in AM to melt the NiTi alloy leads to nickel evaporation, resulting in a chemical change between the batch powder and the additively manufactured part. Therefore, in AM techniques applied to different NiTi alloys, understanding the relationship between the melting strategy and nickel evaporation is crucial during the developing the desired chemical composition of the final-fabricated material. In this study, three NiTi alloys were fabricated using laser powder bed fusion (LPBF) starting from elementally blended Ni and Ti powders. Different melting strategies, including single and multiple melting, were studied in this work. Remelting improved the density and reduced cracking of the AM part. Microscopic observations, using a Scanning Electron Microscope (SEM) with a Backscattered Electron (BSE) detector, showed that the chemical homogeneity of the materials was enhanced by multiple remelting. Pure Ni and Ti were not found in any of the samples, proving that the applied melting strategies ensured good alloying of both powders. Regardless of the number of melting runs, X-ray diffraction (XRD) analysis showed the presence of NiTi (B2) and (B19′) phases, as well as $NiTi_2$, Ni_4Ti_3 and Ni_3Ti precipitates in all samples. The research demonstrated that, during the AM process, and depending on the melting strategy, 1.6–3.0 wt% of nickel evaporates from the material. It was demonstrated that the amount of evaporated nickel increased with the increasing number of melt cycles.

1. Introduction

Additive Manufacturing (AM) technologies provide many benefits and hence components built using this method are being frequently used in all the areas of our lives. Despite their successful development, there is still a strong need to understand and control the phenomenon associated with AM; as this would, in turn, allow a wider use of this technology. Among existing metal AM technologies, laser powder-bed fusion processes (LPBF) are among the most frequently investigated techniques. This is due to the flexibility of the process in the ability to change a large number of process variables and parameters; enabling the successful fabrication of fully dense metal parts with controlled properties [1,2].

NiTi alloys are widely used for many engineering and medical applications owing to their unique shape memory and superelasticity characteristics. However, the specific mechanical properties of NiTi alloys make their machining a challenging task. This significantly reduces their application use and limits the potential of these alloys. According to the previously mentioned difficulties and limitations, the additive manufacturing of NiTi alloys started gaining significant attention because this technology eliminates many of the challenges associated with the conventional methods [3,4]. Plenty of publications show studies on the fabrication of NiTi alloys using many different AM

* Corresponding author.
E-mail address: agnieszka.chmielewska.dokt@pw.edu.pl (A. Chmielewska).

https://doi.org/10.1016/j.mtcomm.2021.103007
Received 13 September 2021; Received in revised form 12 November 2021; Accepted 13 November 2021
Available online 18 November 2021

techniques, such as: the metal injection processes including laser direct energy deposition (LDED) [5], laser direct metal deposition (DMD) [6,7] and laser engineered net shaping (LENS) [8]; and the laser powder-bed fusion (LPBF) processes amongst which selective laser melting (SLM) [9–13] and electron beam melting (EBM) [14,15]. The majority of the research focuses on AM fabrication using pre-alloyed NiTi powders, however, some of the studies implement in-situ alloying using Ni and Ti elemental powders [14,16–19]. *In-situ* alloying is an approach that allows for the synthesis of an alloy from its elemental composition during the manufacturing process. *In-situ* alloying, via AM from elemental powders, is a promising and a cost-effective alternative which offers the flexibility to tailor the composition of the AM part produced. Hence, this method is an easy way to control the material properties or create novel alloys. This route is particularly true and important for producing parts or alloys made of NiTi since their phase transition temperature is highly sensitive to the alloy's composition [14,19–21].

Current research into the AM of NiTi alloys, starting from elemental powders, has been associated with challenges related to the heterogeneity of chemical and phase composition of the fabricated materials. This can be induced by Ni evaporation during the melting process due to its relatively low temperature of evaporation (2732 °C) as compared to that of titanium (3287 °C) [22]. Precise control of the chemical composition of NiTi alloys is extremely important, since the smallest change in the relative Ni or Ti content has a large effect on the transition temperatures; which determine shape memory and superelasticity behaviour [20]. Below the martensite finish temperature (M_f), while above the A_f temperature, NiTi alloys will exhibit superelasticity. The M_s temperature changes by approximately 80 °C for every atomic percent change in Ni content and therefore a great control of the alloying content is required during the manufacturing process [23]. Due to the nature of AM techniques of using high laser energies to consolidate the material, the manufacturing process can lead to evaporation of some alloying elements [24–28]. It is hypothesised that, finding a correlation between the amount of evaporated nickel, as a function of the initial powder composition and manufacturing conditions, would allow for predicting the final chemical composition of the manufactured material. Moreover, it was reported that the homogeneity of the materials fabricated from elemental powders can be improved by remelting each layer [29]. It is important to note that any additional energy input to the material caused by remelting can lead to an increased loss of Ni by evaporation. For this reason, to improve pre-alloying, the influence of manufacturing parameters on the amount of Ni lost by evaporation from the material which are fabricated from elementally blended Ni and Ti powders should be investigated.

This study investigates the level of Ni evaporation in three different NiTi elemental powder blends with the chemical compositions of $Ni_{53}Ti_{47}$ and $Ni_{57}Ti_{43}$ representing the limit values of industrially used NiTi shape memory alloys [30], and $Ni_{55.7}Ti_{43.7}$, which corresponds to pre-alloyed NiTi, used in our previous studies [31]. Moreover, a remelting scanning strategy was applied to increase the homogeneity of the fabricated material. To the best of the authors' knowledge and in relation to the use of LPBF technology in conjunction with elementally blended Ni and Ti powders, the influence of remelting on the chemical composition (Ni:Ti ratio) has not been studied so far. Designing the alloys, and fabricating them from elemental powders, seems to be the promising approach to overcome the difficulties associated with chemical composition changes, and thus, the properties of additively manufactured NiTi alloys. This research will give new insights into new materials that could be developed immediately, and thus eliminating the necessity of the time-consuming and expensive manufacturing of powders. This work would therefore contribute to the faster development of the whole AM industry.

2. Materials and methods

Gas-atomised pure Ni (99.9% in purity, TLS Technik, Germany) and Ti (99.7% in purity, TLS Technik, Germany) powders, having a spherical shape with size below 45 μm were mixed in a tumbling mixer (Turbula, USA) for 2 h and used as powder feedstock. Three different chemical compositions of powder blends were used: $Ni_{53}Ti_{47}$, $Ni_{55.7}Ti_{43.7}$, and $Ni_{57}Ti_{43}$ (wt%). Samples were fabricated with laser powder bed fusion technique (LPBF) using realizer SLM50 (DMG MORI Additive GmbH, Borchen, Germany) machine equipped with a pulsed-wave ytterbium fibre laser having a maximum power of 120 W. Experiments were conducted in an argon atmosphere and with an oxygen content below 0.3 vol%. The NiTi substrate was preheated to 200 °C to decrease the temperature gradient and facilitate the adhesion of the build to it. Samples were fabricated with three different melting strategies and are presented in Fig. 1. The single melting (SM), or first melting, was performed with 30 W of laser power, 500 mm/s of scanning speed, and 30 μm of hatch distance. The remelting, which was done once (Fig. 1. b) or twice (Fig. 2. c) after single melting, was performed with 25 W of laser power, 1000 mm/s of scanning speed, and 30 μm of hatch distance. A layer thickness of 25 μm was used, and to reduce the influence of thermal stresses on samples, scanning rotations of 45° between adjacent layers were applied during fabrication.

The Archimedes standard method was applied to determine the relative density of the fabricated materials. Mass of each sample was measured independently 3 times in air and water using an electronic balance with ± 1 mg of accuracy. The relative density was calculated according to Eq. 1:

$$\rho = \frac{\rho_l}{m_a - m_l} \tag{1}$$

where ρ is relative density, ρ_l is the density of the liquid (water), m_a is the mass of the sample in air and m_l is the mass of the sample in the liquid.

Samples were hot mounted in resin and mechanically polished to be examined under a Zeiss Axio Scope Light Microscope (Germany). The presence of defects, such as porosity and cracks in the samples was assessed. Samples were also examined under a Hitachi SU-8000 (Japan) Scanning Electron Microscope (SEM) in Backscattered Electron (BSE) mode to determine the distribution of Ni and Ti elements.

Phase identification of the manufactured samples was conducted using a Bruker D8 Advance X-ray diffractometer (Bruker, USA) having filtered Cu Kα (λ = 0.154056 nm) radiation and operated at 40 kV and 40 mA. Bruker EVA software and a PDF-2 database (from the International Centre for Diffraction Data) were used to analyse the X-Ray Diffraction (XRD) patterns.

The chemical composition of the fabricated samples was analysed by using a PerkinElmer Optima 8300 (USA) inductively coupled plasma – optical emission spectrometry (ICP-OES). The samples were mineralised in a closed microwave system having an oxidising environment. The prepared samples were analysed by ICP-OES to determine the content of Ni and Ti elements.

Thermal analysis was carried using a DSC 8000 analyser (Perkin-

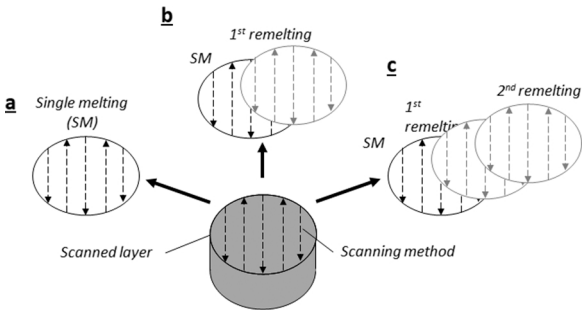

Fig. 1. Schematic illustration of melting strategies: a) laser scanning strategy no. 1: single melting; b) laser scanning strategy no. 2: melting and single remelting; c) laser scanning strategy no. 3: melting and double remelting.

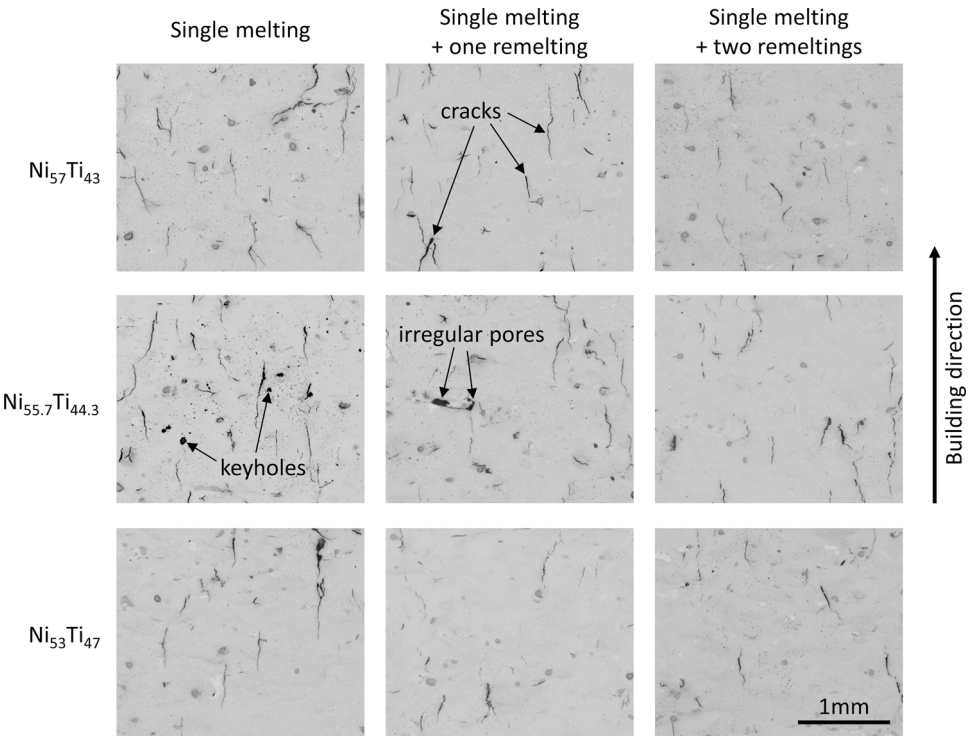

Fig. 2. Light microscopy micrographs of samples manufactured from powders with different initial powder compositions and subjected to different numbers of melt runs. Arrows indicate cracks, irregular pores, and keyholes.

Elmer, USA) which is capable of performing Differential Scanning Calorimetry (DSC) tests. Specimens were tested under an atmosphere of argon gas in the temperature range of 20–120 °C. The heating and cooling rates were of 10 °C/min.

3. Results

3.1. Macroscopic and microscopic observation

Macroscopic observations of each alloy, with an initial powder blend weight ratio of: $Ni_{53}Ti_{47}$, $Ni_{55.7}Ti_{43.7}$, and $Ni_{57}Ti_{43}$, showed that using the same manufacturing parameters ensures good printability. Delamination or macrocracks were not observed for any composition or manufacturing parameters used in this work. The samples were mechanically polished along the Z build direction to assess the presence of micro defects, such as microcracks and pores. As it can be seen in Fig. 2, microcracks along the Z-axis were present in all samples. Other research [32] concluded that this kind of cracks are referred to as 'hot cracks' and will be described in detail in the discussion section of this work. The cross-sections show the presence of spherical and irregular pores. Spherical pores, also referred to as keyhole pores, are created by metal evaporation due to the excess heat input [33,34]. Irregular pores are formed as a result of an insufficient fusion of the subsequent layer of material. As the number of melt runs increases, the number of pores decreases; as does the presence of cracks. The effect is most noticeable for the first remelting when the number of pores and microcracks is significantly reduced. In contrast, after the second remelting run the reduction of pores or cracks number is not that distinct.

3.2. Density measurement

The alloys' densities expressed in g/cm^3 are shown in Fig. 3. The Archimedes density of each sample was measured non-consecutively three times. The results showed that the samples with the highest nickel content (Ni 57%) exhibit the highest density, and the alloy with the lowest initial nickel content had the lowest density (Fig. 3). The

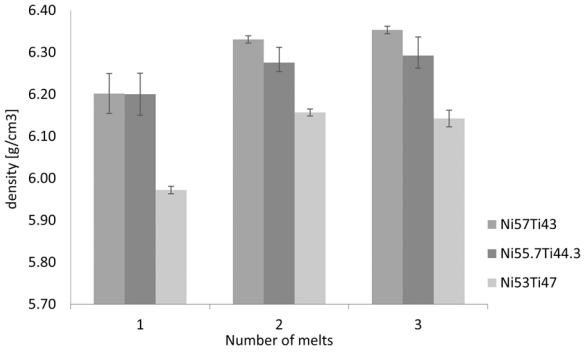

Fig. 3. Relationship between relative density and number of melt runs for NiTi manufactured with elementally blended powders with different chemical compositions. Results represent the mean value of 3 measurements. Error bars present maximum and minimum value of measurements.

density of the fabricated samples increases as the number of melts increases. This confirms earlier assumptions from microscopic observations (Fig. 2) that remelting reduces the closed porosity and cracks that affect the density measurement of the sample by the Archimedes method. There is no clear relationship between the chemical composition of the material or the number of melts and samples density; since the density varies differently for different compositions and numbers of melts. The greatest increase in density occurs after the second melting; the third melting does not significantly affect the density. This also confirms microscopic observations that the number of pores decreases most after the second melting and slightly after the third melting.

3.3. Scanning electron microscopy - backscattering electrons

Fusion zones, in the manufactured samples, were observed in the BSE SEM images (Fig. 4). The bright areas are undiffused Ni-rich phases, while the dark shaded are Ti-rich regions. It can be noted that remelted

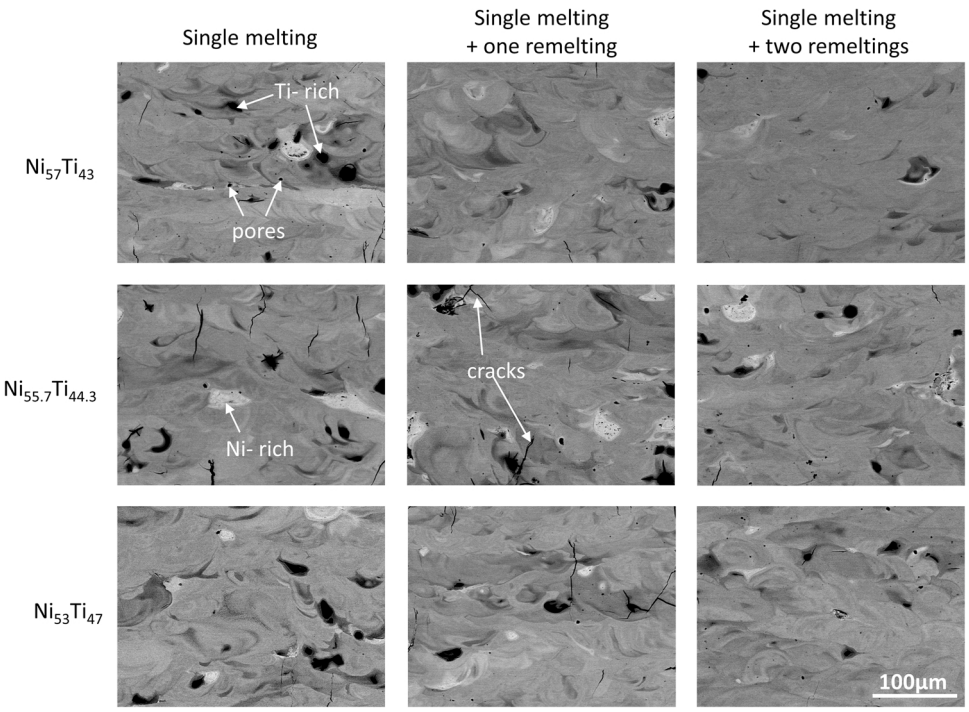

Fig. 4. BSE SEM micrographs of samples manufactured from powders with different initial powders compositions and subjected to different numbers of meltings. Dark and light shaded areas are titanium- and nickel-rich, phases respectively. Arrows indicate cracks, pores and Ti- and Ni-rich areas.

samples have a more homogenous microstructure in terms of Ni and Ti distribution; with the homogeneity increasing with an increase in the number of melt runs. Higher homogeneity is indicated by the lower phase contrast in the BSE SEM images.

3.4. X-ray diffraction

The phase composition of the manufactured alloy was determined by XRD analysis and Fig. 5 presents the patterns of all manufactured samples. The results indicate the presence of NiTi (B2) austenite phase, having a cubic structure, and (B19′) martensite phase, having monoclinic structure. $NiTi_2$, Ni_4Ti_3 and Ni_3Ti phases were identified in all samples. There is no evidence of free nickel and titanium peaks; proving that both elements have been thoroughly alloyed. Variation in the $NiTi_2$ and NiTi B19′ peaks intensities, which overlap each other, was found. The intensities of the $NiTi_2$ and NiTi B19′ peaks are shown to increase with a decrease in the nickel content of the pre-printed powder composition.

3.5. Inductively coupled plasma optical emission spectroscopy (ICP OES)

For each sample, the chemical composition was analysed using inductively coupled plasma-optical emission spectrometry (ICP-OES). The analysis was performed to determine changes in the chemical composition (nickel evaporation) depending on the chemical composition of the initial powder blend, as well as the number of melts. The ICP-OES data showed that the amount of nickel in the material decreases with an increasing number of melt runs (Fig. 6). However, the decrease in nickel content with the number of melt runs was not uniform for each of the blends.

3.6. Differential scanning calorimetry (DSC)

Fig. 7 presents the DSC curves of samples manufactured with different compositions and melting strategies. Due to the heterogeneous microstructure of the materials the DSC peaks are very wide, and it is difficult to determine the exact temperature of the start and end of both

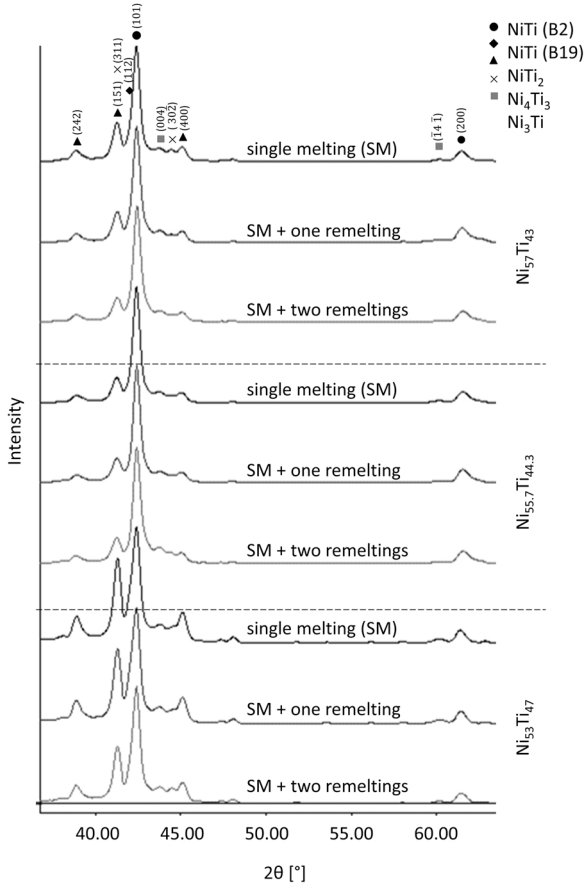

Fig. 5. The XRD diffractograms of samples fabricated from powders with different initial powders compositions and subjected to different number of melt runs.

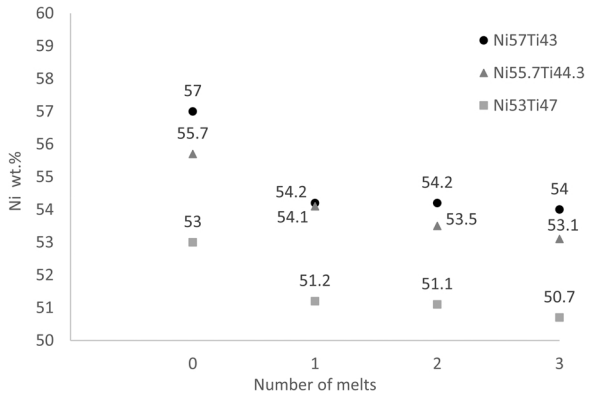

Fig. 6. Results of ICP OES analysis of samples fabricated from powders with different initial powders compositions and subjected to different numbers of melt runs; 0 refers to pre-printed powder; 1- single melting run; 2- single melting run and one remelting run; 3- single melting run and two remelting runs; the measurement error was ± 0.1 wt%.

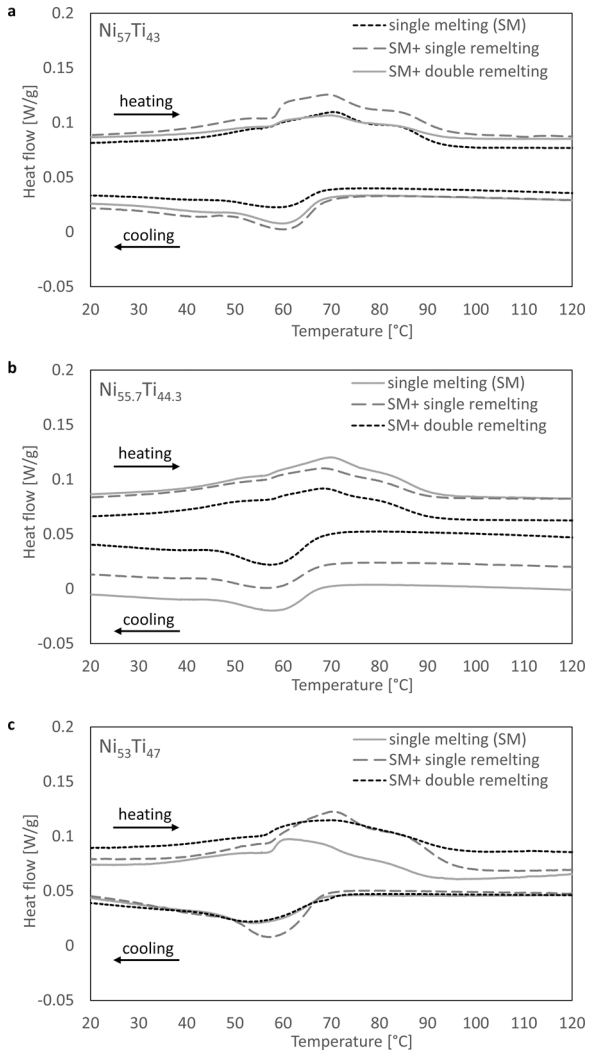

Fig. 7. The DSC curves of samples manufactured with different composition and melting strategies: a) $Ni_{53}Ti_{47}$; b) $Ni_{55.7}Ti_{43.7}$ and c) $Ni_{57}Ti_{43}$.

the austenitic and martensitic transition. However, it can be found that the martensitic transition temperatures decrease to about 5–8 °C with the decreasing content of Ni for different blends. However, for the blends with the same initial powder composition and produced using different melting strategies (number of melts), the differences in transition temperatures are barely noticeable and have a range of about 1–2 °C.

4. Discussion

The research focused on determining the value of nickel evaporation from three NiTi powder mixtures with different chemical compositions: $Ni_{53}Ti_{47}$, $Ni_{55.7}Ti_{43.7}$, and $Ni_{57}Ti_{43}$ (wt%) fabricated by LPBF with three different melting strategies. Moreover, the influence of multiple melting on the alloy microstructure was shown. Microscopic observation has revealed the presence of microcracks along the building direction (Fig. 2). The high thermal gradients associated with the LPBF process contribute to the formation of residual stresses, and in turn, induce large susceptibility to hot cracking [32,35,36]. Two mechanisms of hot cracking can be distinguished: solidification cracking and liquidation cracking. Solidification cracking occurs in the fusion zone when the material is in a semi-solid state during laser melting, which means that it consists of a partially solidified material with a non-solidified liquid entrapped in between. Solidification of the entrapped liquid induces tensile residual stresses, which in turn initiates cracking. This phenomenon was observed for materials in which some phases had a much lower melting point than other components [37]. This problem applies to the Ni and Ti powder blends since titanium has a much higher melting point than nickel; which are 1670 °C and 1455 °C, respectively. Furthermore, the results of BSE images (Fig. 4) and XRD (Fig. 5) revealed the existence of various phases in the manufactured samples, including the NiTi phase, with a melting point of 1310 °C, and a $NiTi_2$ phase with a much lower melting point of 984 °C. Thus, due to the presence of various phases with different melting temperatures within the material, solidification cracking may occur. Liquation cracking occurs in the heat-affected zone where phases with low melting points are presented, such as eutectics and zones with chemical segregation. When the material is heated, a thin film of liquid material forms in the heat-affected zone, which eventually shrinks as it solidifies and promotes crack formation [32,38–40].

The number of cracks in samples subjected to additional melting (remelted) is reduced, which may be the result of filling cracks with liquid metal during remelting [32]. Significant differences in the reduction of microcracks are observed after the second melting, while the number of microcracks does not change distinctly after the third melting. This phenomenon may be evidenced by the fact that some of the microcracks were filled with liquid metal but some of them remained. This is due to the high internal stresses in the material generated by multiple remelting. The reduction in the number of cracks and pores also resulted in a density increase (Fig. 3).

Although both components were not thoroughly blended (Fig. 4), no peaks of free nickel and titanium were observed in the XRD traces (Fig. 5). A recent study [8] demonstrated that martensitic (B19′) and austenitic (B2) phases coexist in additively manufactured NiTi. The B2 phase is known to be stable at higher temperatures, while the B19′ phase exists at lower temperatures. However, their transition temperatures depend on the chemical composition of the alloy. The lower the Ni content, the lower the transition temperature. This means, that at the same temperature the nickel-rich B2 phase can coexist simultaneously with the titanium-rich B19′ phase within one material with areas having different Ni/Ti contents. In this study, BSE SEM observations showed heterogeneity in the alloying of both elements, and therefore, Ni and Ti-rich areas are observed within the microstructure. Furthermore, the increase in $NiTi_2$/NiTi (B19′) peak intensity was observed for samples with the lowest Ni content in the initial powder blend. Since peaks corresponding to NiTi (B19′) and $NiTi_2$ overlap each other, it is not possible to unequivocally determine which of those phases has a greater impact on the increase of that specific peak intensity. Moreover, it is possible, that both phases contribute to the peak growth due to the

presence of two different phenomena. Firstly, as the Ni content decreases, the likelihood of $NiTi_2$ phase formation increases due to the lack of sufficient nickel atoms to form the NiTi phase. Secondly, a decrease in Ni content also causes a decrease in the martensitic transition temperature. Accordingly, the probability of the formation of more martensite than austenite in the material increases. The nickel content in samples $Ni_{57}Ti_{43}$ and $Ni_{55.7}Ti_{43.7}$ is more similar to each other; 57% and 55.7% of Ni respectively. Thus, the differences between their peaks are lower, than that of the $Ni_{53}Ti_{47}$ samples, with a nickel content of 53% [41]. The intensity of $NiTi_2$ and NiTi (B19′) diffraction peaks is the highest for 7–9 samples, which have significantly lower amounts of nickel.

The ICP OES results showed changes in Ni content in samples of different compositions subjected to a different number of melts (Fig. 6). In all samples there was a decrease in the amount of nickel from the initial powder blend composition. Depending on the initial powder blend composition and melting strategy, the amount of evaporated Ni ranges from 1.6 to 3 wt%. The content of Ni decreases with the increasing number of melts. During the subsequent laser melting with a high-power laser. the material is reheated and melted multiple times, hence, there is a higher probability for Ni evaporation. Consequently, the more times the material is remelted, the more Ni would evaporate. It would be beneficial to predict the amount of evaporated nickel during LPBF manufacturing depending on the composition of the batch powder and the scanning and melting strategy used during the manufacturing process. Thus, to obtain a desired final alloy composition, the initial powder composition and manufacturing strategy must be developed separately.

DSC plots, shown in Fig. 7, are not uniform, and multiple small peaks are observed. In general, the existence of an additional peak before the austenitic and martensitic transition is related to the presence of the R phase, which is the intermediate phase between martensite and austenite [42]. Nevertheless, in the presented DSC results, multiple small additional peaks are observed along the entire length of the transition peak. Therefore, it can be concluded that these peaks are not related to the presence of R phase and might be generated by heterogeneity in Ni and Ti distribution in the NiTi phase. It can also be seen that the peaks of austenitic and martensitic transition are wide, and it is difficult to precisely determine the start and finish transition temperatures. Li et al. [38] have reported that the peak width is related to the inhomogeneity of the B19′ phase. It is possible, that the range of the transition temperatures extends over a wider area, while B19′/B2 phases show chemical inhomogeneities in the Ti/Ni content; since the NiTi phase can be composed of 53–57 wt% of Ni. Nevertheless, a slight shift of the value of the transition temperatures is observed in the samples with different initial powder blend compositions and this is due to the reduction in nickel content. It was found that with the decrease in Ni content in various blends, the transition temperature decreased by about 5–8 °C, while for the blends with the same initial powder composition and produced using different melting strategies (number of melts), the transition temperature decreases by only about 1–2 °C. It is well known that a 1 at% change in nickel content changes the transition temperature by about 80 °C [23]; however, such a large change in transition temperature was not noticeable in the studied AM produced samples of this work. This is because the microstructure is very heterogeneous, resulting in a wide DSC peak and the inability to accurately determine the start and end transition temperatures. Therefore, it would be necessary to homogenise the microstructure by a post-additive manufacturing heat treatment in order to be able to more accurately define the start and finish martensitic and austenitic transition temperatures.

5. Conclusions

Three NiTi powder blends with chemical compositions of $Ni_{53}Ti_{47}$, $Ni_{55.7}Ti_{43.7}$, and $Ni_{57}Ti_{43}$ (wt%) were melted by LPBF using three different melting strategies. The same manufacturing parameters applied to all powder blends allowed each sample to be successfully fabricated. Ni evaporation from the manufactured samples was studied, and the amount of nickel that evaporates during the production process ranges from 1.6 to 3.0 wt%. This depends on the initial powder's chemical composition and the number of melts. It was demonstrated that the amount of evaporated nickel increases with increasing number of melt cycles. Furthermore, an increase in the number of melt cycles reduces the number of cracks and pores and increases the chemical homogeneity of the alloy. Nevertheless, multiple meltings can still generate high residual stresses and result in crack formation. Thus, the number of remelting cycles must be precisely defined to increase the chemical homogeneity and density of the material and prevent cracking. Due to the large heterogeneity of the chemical composition of the manufactured materials, it was difficult to accurately determine the start and final transition temperatures of martensite and austenite. Therefore, homogenisation of the chemical composition would be necessary to precisely define the influence of different melting strategies on the transition temperatures, and hence, thermomechanical properties of the material. Since remelting does not eliminate the problem of heterogeneity an additional heat treatment would be required and further investigated. The presented results are very promising for in situ alloying in additive manufacturing and could provide valuable information for designing the batch material's chemical composition to obtain the desired chemical composition of the fabricated alloy.

Declaration of Competing Interest

The authors declare that they have no known competing financial interests or personal relationships that could have appeared to influence the work reported in this paper.

Acknowledgments

Bartłomiej Wysocki acknowledges the grant provided by the Kosciuszko Foundation (www.thekf.org) -the American Centre of Polish Culture.

References

[1] I. Gibson, D. Rosen, B. Stucker. Additive Manufacturing Technologies 3D Printing, Rapid Prototyping, and Direct Digital Manufacturing, Second ed.,, Springer, 2015, https://doi.org/10.2495/SDP-V9-N5-658-668.
[2] A. Bandyopadhyay, S. Bose. Additive Manufacturing, First ed.,, CRC Press Taylor & Francis Group, Boca Raton, 2015, https://doi.org/10.1201/b18893.
[3] M. Mahmoudi, G. Tapia, B. Franco, J. Ma, R. Arroyave, I. Karaman, A. Elwany, On the printability and transformation behavior of nickel-titanium shape memory alloys fabricated using laser powder-bed fusion additive manufacturing, J. Manuf. Process. 35 (2018) 672–680, https://doi.org/10.1016/j.jmapro.2018.08.037.
[4] M. Elahinia, N. Shayesteh Moghaddam, M. Taheri Andani, A. Amerinatanzi, B. A. Bimber, R.F. Hamilton, Fabrication of NiTi through additive manufacturing: a review, Prog. Mater. Sci. 83 (2016) 630–663, https://doi.org/10.1016/j.pmatsci.2016.08.001.
[5] B.A. Bimber, R.F. Hamilton, J. Keist, T.A. Palmer, Anisotropic microstructure and superelasticity of additive manufactured NiTi alloy bulk builds using laser directed energy deposition, Mater. Sci. Eng. A 674 (2016) 125–134, https://doi.org/10.1016/j.msea.2016.07.059.
[6] K. Malukhin, K. Ehmann, Material characterization of NiTi based memory alloys fabricated by the laser direct metal deposition process, J. Manuf. Sci. Eng. 128 (2006) 691, https://doi.org/10.1115/1.2193553.
[7] S. Khademzadeh, S. Carmignato, N. Parvin, F. Zanini, P.F. Bariani, Micro porosity analysis in additive manufactured NiTi parts using micro computed tomography and electron microscopy, Mater. Des. 90 (2016) 745–752, https://doi.org/10.1016/j.matdes.2015.10.161.
[8] J.J. Marattukalam, A.K. Singh, S. Datta, M. Das, V.K. Balla, S. Bontha, S. K. Kalpathy, Microstructure and corrosion behavior of laser processed NiTi alloy, Mater. Sci. Eng. C 57 (2015) 309–313, https://doi.org/10.1016/j.msec.2015.07.067.
[9] T. Gustmann, F. Gutmann, F. Wenz, P. Koch, R. Stelzer, W.G. Drossel, H. Korn, Properties of a superelastic NiTi shape memory alloy using laser powder bed fusion and adaptive scanning strategies, Prog. Addit. Manuf. 5 (2020) 11–18, https://doi.org/10.1007/s40964-020-00118-6.
[10] T. Bormann, B. Müller, M. Schinhammer, A. Kessler, P. Thalmann, M. De Wild, Microstructure of selective laser melted nickel-titanium, Mater. Charact. 94 (2014) 189–202, https://doi.org/10.1016/j.matchar.2014.05.017.

[11] A. Jahadakbar, N. Shayesteh Moghaddam, A. Amerinatanzi, D. Dean, M. Elahinia, Mechanical evaluation of the SLM fabricated, stiffness-matched, mandibular bone fixation plates, Proc. SPIE 1059610 (2018) 31, https://doi.org/10.1117/12.2300740.
[12] M. Speirs, X. Wang, S. Van Baelen, A. Ahadi, S. Dadbakhsh, J.-P. Kruth, J. Van Humbeeck, On the transformation behavior of NiTi shape-memory alloy produced by SLM, Shape Mem. Superelast. 2 (2016) 310–316, https://doi.org/10.1007/s40830-016-0083-y.
[13] M.R. Karamooz-Ravari, M. Taheri Andani, M. Kadkhodaei, S. Saedi, H. Karaca, M. Elahinia, Modeling the cyclic shape memory and superelasticity of selective laser melting fabricated NiTi, Int. J. Mech. Sci. 138–139 (2018) 54–61, https://doi.org/10.1016/j.ijmecsci.2018.01.034.
[14] C. Wang, X.P. Tan, Z. Du, S. Chandra, Z. Sun, C.W.J. Lim, S.B. Tor, C.S. Lim, C. H. Wong, Additive manufacturing of NiTi shape memory alloys using pre-mixed powders, J. Mater. Process. Technol. 271 (2019) 152–161, https://doi.org/10.1016/j.jmatprotec.2019.03.025.
[15] Q. Zhou, M.D. Hayat, G. Chen, S. Cai, X. Qu, H. Tang, P. Cao, Selective electron beam melting of NiTi: Microstructure, phase transformation and mechanical properties, Mater. Sci. Eng. A 744 (2019) 290–298, https://doi.org/10.1016/j.msea.2018.12.023.
[16] C. Zhao, H. Liang, S. Luo, J. Yang, Z. Wang, The effect of energy input on reaction, phase transition and shape memory effect of NiTi alloy by selective laser melting, J. Alloy. Compd. 817 (2020), 153288, https://doi.org/10.1016/j.jallcom.2019.153288.
[17] P. Stoll, A. Spierings, K. Wegner, SLM processing of elementally blended NiTi shape memory alloy, Procedia CIRP 95 (2020) 121–126, https://doi.org/10.1016/j.procir.2020.02.250.
[18] B. Zhang, J. Chen, C. Coddet, Microstructure and transformation behavior of in-situ shape memory alloys by selective laser melting Ti-Ni mixed powder, J. Mater. Sci. Technol. 29 (2013) 863–867, https://doi.org/10.1016/j.jmst.2013.05.006.
[19] M.H. Mosallanejad, B. Niroumand, A. Aversa, A. Saboori, In-situ alloying in laser-based additive manufacturing processes: a critical review, J. Alloy. Compd. 872 (2021), 159567, https://doi.org/10.1016/j.jallcom.2021.159567.
[20] J. Frenzel, E.P. George, A. Dlouhy, C. Somsen, M.F.X. Wagner, G. Eggeler, Influence of Ni on martensitic phase transformations in NiTi shape memory alloys, Acta Mater. 58 (2010) 3444–3458, https://doi.org/10.1016/j.actamat.2010.02.019.
[21] A. Katz-Demyanetz, A. Koptyug, V.V. Popov, In-situ alloying as a novel methodology in additive manufacturing, In: Proceedings of the 2020 IEEE 10th International Conference "Nanomaterials Appl. Prop. N. 2020. 2020 26–29. ⟨https://doi.org/10.1109/NAP51477.2020.9309652⟩.
[22] P.R. Halani, Y.C. Shin, In situ synthesis and characterization of shape memory alloy nitinol by laser direct deposition, Metall. Mater. Trans. A Phys. Metall. Mater. Sci. 43 (2012) 650–657, https://doi.org/10.1007/s11661-011-0890-x.
[23] M. Mouis, E. Chávez-Ángel, C. Sotomayor-Torres, F. Alzina, M.V. Costache, A.G. Nassiopoulou, K. Valalaki, E. Hourdakis, S.O. Valenzuela, B. Viala, D. Zakharov, Ahopelto, A. Shchepetov, J. Ahopelto, Thermal Energy Harvesting System, in: F. Balestra (Ed.), Beyond C. Nanodevices 1, First, ISTE Ltd and John Wiley & Sons, Inc., 2014, p. 194. ⟨https://doi.org/10.1002/9781118984772⟩.
[24] A. Zhukov, B. Barakhtin, I. Shakirov, V. Bobyr, The emergence of inhomogeneity in the chemical composition of powder applicable for manufacturing products by additive technologies, Procedia Manuf. 36 (2019) 19–25, https://doi.org/10.1016/j.promfg.2019.08.004.
[25] J. Sedlak, D. Rican, M. Piska, L. Rozkosny, Study of materials produced by powder metallurgy using classical and modern additive laser technology, Procedia Eng. 100 (2015) 1232–1241, https://doi.org/10.1016/j.proeng.2015.01.488.
[26] I. Voiculescu, V. Geanta, I.M. Vasile, E.F. Binchiciu, R. Winestoock, Chemical elements diffusion in the stainless steel components brazed with Cu-Ag alloy, in: Proceedings of the IOP Conference Series Materials Science Engineering, 2016, pp. 1–8. ⟨https://doi.org/10.1088/1757–899X/133/1/012014⟩.
[27] A. Klassen, T. Scharowsky, C. Körner, Evaporation model for beam based additive manufacturing using free surface lattice Boltzmann methods, J. Phys. D Appl. Phys. 47 (2014) 1–12, https://doi.org/10.1088/0022-3727/47/27/275303.
[28] M. Doubenskaia, A. Domashenkov, I. Smurov, P. Petrovskiy, Study of selective laser melting of intermetallic TiAl powder using integral analysis, Int. J. Mach. Tools Manuf. 129 (2018) 1–14, https://doi.org/10.1016/j.ijmachtools.2018.02.003.
[29] H. Zhang, Y. Zhao, S. Huang, S. Zhu, F. Wang, D. Li, Manufacturing and analysis of high-performance refractory high-entropy alloy via selective laser melting (SLM), Materials 12 (2019), https://doi.org/10.3390/ma12050720.
[30] H. Morawiec, Metale z pamięcia kształtu i ich zastosowanie, Wydawnictwo Uniwersytetu Śląskiego, Katowice, 2014.
[31] A. Chmielewska, A. Jahadakbar, B. Wysocki, M. Elahinia, W. Święszkowski, D. Dean, Chemical polishing of additively manufactured, porous, nickel–titanium skeletal fixation plates, 3D print, Addit. Manuf. (2021) 10, https://doi.org/0.1089/3dp.2020.0209.
[32] F.M. Ghaini, M. Sheikhi, M.J. Torkamany, J. Sabbaghzadeh, The relation between liquation and solidification cracks in pulsed laser welding of 2024 aluminium alloy, Mater. Sci. Eng. A 519 (2009) 167–171, https://doi.org/10.1016/j.msea.2009.04.056.
[33] J. Trapp, A.M. Rubenchik, G. Guss, M.J. Matthews, In situ absorptivity measurements of metallic powders during laser powder-bed fusion additive manufacturing, Appl. Mater. Today 9 (2017) 341–349, https://doi.org/10.1016/j.apmt.2017.08.006.
[34] B. Liu, G. Fang, L. Lei, An analytical model for rapid predicting molten pool geometry of selective laser melting (SLM), Appl. Math. Model. 92 (2021) 505–524, https://doi.org/10.1016/j.apm.2020.11.027.
[35] T. Böllinghaus, H. Herold, Hot Cracking Phenomena in Welds, Springer, Berlin, 2005.
[36] N.T. Aboulkhair, M. Simonelli, L. Parry, I. Ashcroft, C. Tuck, R. Hague, 3D printing of aluminium alloys: additive manufacturing of aluminium alloys using selective laser melting, Prog. Mater. Sci. 106 (2019), 100578, https://doi.org/10.1016/j.pmatsci.2019.100578.
[37] S. Dadbakhsh, R. Mertens, K. Vanmeensel, J. Vleugels, J. Van Humbeeck, J. P. Kruth, In situ alloying and reinforcing of Al6061 during selective laser melting, Procedia CIRP 74 (2018) 39–43, https://doi.org/10.1016/j.procir.2018.08.009.
[38] S. Li, H. Hassanin, M.M. Attallah, N.J.E. Adkins, K. Essa, The development of TiNi-based negative Poisson's ratio structure using selective laser melting, Acta Mater. 105 (2016) 75–83, https://doi.org/10.1016/j.actamat.2015.12.017.
[39] N. Kalentics, N. Sohrabi, H.G. Tabasi, S. Griffiths, J. Jhabvala, C. Leinenbach, A. Burn, R.E. Logé, Healing cracks in selective laser melting by 3D laser shock peening, Addit. Manuf. 30 (2019), 100881, https://doi.org/10.1016/j.addma.2019.100881.
[40] X. Zhang, H. Chen, L. Xu, J. Xu, X. Ren, X. Chen, Cracking mechanism and susceptibility of laser melting deposited Inconel 738 superalloy, Mater. Des. 183 (2019), 108105, https://doi.org/10.1016/j.matdes.2019.108105.
[41] J.P. Oliveira, A.J. Cavaleiro, N. Schell, A. Stark, R.M. Miranda, J.L. Ocana, F.M. Braz Fernandes, Effects of laser processing on the transformation characteristics of NiTi: a contribute to additive manufacturing, Scr. Mater. 152 (2018) 122–126, https://doi.org/10.1016/j.scriptamat.2018.04.024.
[42] D.C. Lagoudas, Shape Memory Alloys- Modeling and Engineering Applications, Springer, 2008, https://doi.org/10.1002/0471732877.emd002.